Korean J. Chem. Eng., **30**(1), 33-44 (2013)
DOI: 10.1007/s11814-012-0117-x

Non-Newtonian power-law flow across a confined triangular bluff body in a channel

Amit Kumar Dhiman† and Shailesh Kumar

Department of Chemical Engineering, Indian Institute of Technology Roorkee, Roorkee 247 667, India
(*Received 14 April 2012 • accepted 19 July 2012*)

Abstract−Wall effects on the flow of incompressible non-Newtonian power-law fluids across an equilateral triangular cylinder confined in a horizontal plane channel have been investigated for the range of conditions: Reynolds number, Re=1-40, power-law index, n=0.4-1.8 (covering shear-thinning, Newtonian and shear-thickening behaviors) and blockage ratio=0.125-0.5. Extensive numerical results on flow pattern, wake/recirculation length, individual and overall drag coefficients, variation of pressure coefficient on the surface of the triangular cylinder and so forth are reported to elucidate the combined effect of power-law index, blockage ratio and Reynolds number. The size of vortices decreases with an increase in the value of the blockage ratio and/or power-law index. For a fixed value of the Reynolds number, individual and overall drags decrease with decrease in power-law index and/or blockage ratio in steady confined flow regime. Simple correlations of wake length and drag are also obtained for the range of settings considered.

Key words: Non-Newtonian Fluids, Drag, Wake Length, Reynolds Number, Power-law Index

INTRODUCTION

Flow past bluff bodies has been investigated both numerically and experimentally because of the large number of engineering applications such as electronic cooling, compact heat exchange systems, offshore structures, flame stabilizers in combustion chambers, aerodynamic fields, flow meters and so forth. Additional applications are found in polymer and food industries, and chemical and process engineering applications often exhibit the class of structured fluids which display shear-thinning and shear-thickening behaviors under appropriate conditions [1]. Despite their wide occurrence, more information is available on the flow of non-Newtonian power-law fluids past a circular cylinder [2-16] and a square cylinder [17-23] in both confined and unconfined configurations. While there has been only one recent study documented on the flow of such non-Newtonian fluids past a bluff body of triangular cross-section in the unconfined domain [24], and no work is available on the power-law fluids across a confined triangular cylinder in a channel. The present work aims to fill this gap in the existing literature as the wall effects play an important role on the flow and heat transfer characteristics over a bluff body. However, it is useful to first briefly recount the corresponding body of knowledge available for the flow of Newtonian fluids over a triangular obstacle, as this facilitates the subsequent discussion for non-Newtonian fluids.

PREVIOUS WORK

In the literature, sufficient accounts of numerical studies of the flow of Newtonian fluids over a triangular cylinder in confined configuration are available in both steady and unsteady regimes. Abbassi et al. [25] carried out the two-dimensional numerical investigations to the mixed (free and forced) convection of air in a horizontal channel with a built-in triangular prism for the fixed value of Re=100, Pr=0.71 and $0 \le Gr \le 1.5 \times 10^4$. The effects of thermal buoyancy lead to a slight increase in the frequency of the vortex shedding and the Von Kármán Street favors the formation of convective cells. Also, the presence of the triangular prism leads to a significant increase in the value of the time-averaged Nusselt number (more than 44%). Subsequently, Abbassi et al. [26] carried out a 2-D numerical investigation of the forced convection in the horizontal channel with a built-in triangular prism for the Reynolds number range Re=20-250 and the Prandtl number of 0.71 for the fixed value of the blockage ratio of 0.25. They observed the transition from symmetric to unsteady periodic flow at Re=45, and for the symmetric flow (Re<45) the presence of the triangular prism has a local weak effects on the heat transfer and the flow pattern. But in periodic flow (Re≥45) an augmentation in the value of the space and time-averaged Nusselt number of 85% has been recorded at Re=250. De and Dalal [27] studied the 2-D unsteady flow and heat transfer past an equilateral triangular cylinder placed in a horizontal channel for the range of conditions as $80 \le Re \le 200$ and blockage ratio $1/12 \le \beta \le 1/3$. The St-Re relationship has a flat maximum around Re=130 for $\beta < 1/6$; whereas, it increases monotonically for $\beta \ge 1/6$ with Re and for Re>130. They also reported that the blockage ratio has negligible effect on the time-averaged overall Nusselt number. Chattopadhyay [28] studied the heat transfer in a channel in the presence of a triangular prism at very high Reynolds number of 40000 for a fixed aspect ratio of channel to the prism element of 4. They showed that in the presence of a triangular element, heat transfer in a channel is augmented by around 15%. Dhiman and Srikanth [29] studied the steady flow of Newtonian fluid across an equilateral triangular cylinder placed in a horizontal channel for Re=20 and 40 for a fixed blockage ratio of 0.25. They reported that the total drag coefficient decreases with increasing value of the Reynolds number; however, the wake length increases with increasing value of Reynolds number. Farhadi et al. [30] studied the effect of wall proximity of a triangular obstacle on the unsteady fluid flow and heat transfer in a horizontal plane channel

†To whom correspondence should be addressed.
E-mail: dhimuamit@rediffmail.com, amitdfch@iitr.ernet.in

for Re=100, 250, 350 and 450 for a fixed value of the Prandtl number of 0.71. By approaching triangular cylinder towards the wall, vortex shedding suppresses and subsequently the heat transfer rate decreases at low Reynolds number. However, the variation of vortex formation has a more significant suppression effect on the skin friction coefficient than the Nusselt number. Subsequently, Srikanth et al. [31] investigated the flow and heat transfer around a long conned equilateral triangular cylinder for the Reynolds number range Re= 1-80 and Prandtl number of 0.71 for a fixed value of the blockage ratio of 0.25. A critical value of the Reynolds number (i.e., transition to unsteady) has been observed between Re=58 and 59. The total drag coefficient decreases with increasing value of the Reynolds number. On the other hand, the wake length and the average Nusselt number increase with increasing value of the Reynolds number. Recently, Ali et al. [32] did experimental investigations on the forced convection heat transfer from the outer surface of horizontal triangular cylinders in cross-flow of air at very large values of Re. Four equilateral triangular cylinders were used with cross-section side lengths of 0.03, 0.05, 0.08 and 0.12 m, corresponding to the values of blockage ratio of 0.066, 0.11, 0.175 and 0.263, respectively. The overall average Nusselt numbers were obtained for transition to turbulent regime. Empirical correlations were also obtained for the overall average Nusselt number for the two positions of the triangular cylinders.

On the other hand, for unconfined flow and heat transfer across a triangular cylinder, sufficient information is now available in the literature on the Newtonian fluid flow and heat transfer around a long triangular cylinder in both steady and unsteady regimes (De and Dalal [33]; Dalal et al. [34]; Dhiman [35], Dhiman and Shyam [36], Zeitoun et al. [37] and Prhashanna et al. [24], for instance). De and Dalal [33] carried out the 2-D numerical investigations of the fluid flow across an equilateral triangular cylinder in the unconfined space in the Reynolds number range 10≤Re≤250. They studied global modes in the wake flow, and the value of critical Reynolds number for the triangular cylinder is reported to be 39.9. Subsequently, Dalal et al. [34] proposed a novel finite-volume formulation for unsteady solutions on complex geometries. They presented a computational study of 2-D laminar flow and heat transfer past a triangular cylinder in free stream for Re range 10≤Re≤200 at Pr= 0.71. The time-averaged Nusselt number increases quasi-linearly with increasing value of the Reynolds number. However, limited information is available on the variation of the local Nusselt number, and no information in available on the temporal variation of the Nusselt number with Reynolds number. Recently, Dhiman [35] investigated the fluid flow and heat transfer over an equilateral triangular cylinder in the steady unconfined cross-flow regime for the range of conditions: Re=10, 25 and Pr=0.7. The individual and total drag coefficients decrease with increasing value of the Reynolds number. However, the average Nusselt number increases with increasing value of the Reynolds number. Dhiman and Shyam [36] studied the unsteady heat transfer from an equilateral triangular cylinder for the Reynolds numbers of 100 and 130 for the fixed value of the Prandtl number of 0.7. The time-averaged Nusselt number increases with increasing value of the Reynolds number. Zeitoun et al. [37] did a 2-D numerical study around an equilateral triangular cylinder of different side dimensions and configurations under laminar conditions (Re≤200). The critical Re for both vertex facing and base facing flows was reported as 38.03 and 34.7, respectively. Recently, Prhashanna et al. [24] numerically investigated the 2-D laminar flow of power-law fluids over an equilateral triangular cylinder to elucidate the role of power-law index (0.2≤n≤1.8) on the critical Re denoting the onset of flow separation and of vortex shedding. The results are presented for both orientations (apex facing upstream and downstream directions) by using Fluent. The detailed results are presented for steady shear-thinning and Newtonian fluids for the following range of conditions: 0.2≤n≤1, 1≤Re≤30 and 1≤Pr≤ 100. The pressure and total drag coefficients decrease with Re, and the Nusselt number increases with Pr and Re irrespective of power-law index. The effect of power-law index gradually diminishes with increasing Re.

From the above discussion, it can be summarized that flow and heat transfer across the long triangular obstacle are usually studied for Newtonian fluids (n=1) in both confined and unconfined domains in both steady and unsteady regimes. Only Prhashanna et al. [24] investigated the flow of power-law fluids across an equilateral triangular obstacle in the unconfined domain. Wall effects on momentum and heat transfer phenomena of a bluff body of triangular cross-section are of particular relevance as discussed in the beginning, and still no work is available on the flow of non-Newtonian power-law fluids (n≠1) in a channel with a built-in triangular cylinder. Thus, the aim of this study is to investigate the effect of wall proximity on the flow of non-Newtonian power-law fluids across a triangular cylinder placed in a 2-D horizontal plane channel. In particular, the focus of this study is to understand flow structures, drag coefficient, wake formation and recirculation length over an equilateral triangular cylinder for power-law fluids at low Reynolds numbers. The numerical results are presented for power-law fluids for Re=1-40 for the three values of blockage ratio of 0.125, 0.25, 0.5 at different value of power-law index of 0.4, 0.6, 1, 1.4 and 1.8 (there by covering shear-thinning (n<1), Newtonian (n=1) and shear-thickening (n>1) behaviors).

PROBLEM STATEMENT AND MATHEMATICAL FORMULATION

The 2-D flow of incompressible non-Newtonian power-law fluids in a horizontal plane channel with an equilateral triangular cylin-

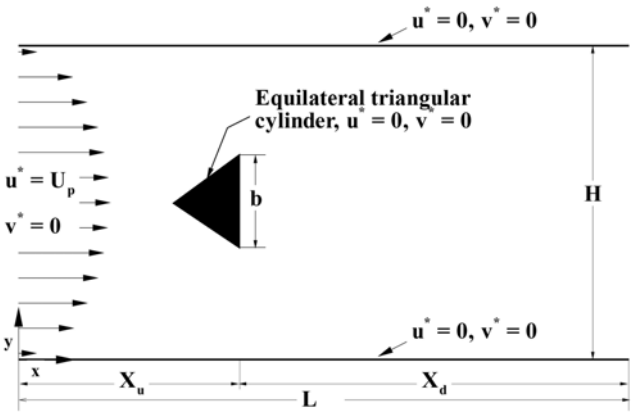

Fig. 1. Schematic of the confined flow around a triangular obstacle in a channel.

der placed symmetrically on the centerline is considered, as shown in Fig. 1. The equilateral triangular cylinder with side b (also the non-dimensional length scale) is exposed to a fully developed velocity field with an average velocity of U_{avg} (also the non-dimensional velocity scale) at the channel inlet. The non-dimensional upstream distance between the inlet plane and the rear surface of the triangular cylinder is X_u/b and the non-dimensional downstream distance between the rear surface of the triangular cylinder and the exit plane is X_d/b with the total non-dimensional length of the computational domain is L/b in the axial direction. The non-dimensional vertical distance between the upper and lower bounding walls is H/b in the lateral direction. In this study, the blockage ratio (BR) is defined as β=b/H.

The fully developed velocity profile for the laminar flow of power-law fluids in a channel is given as [38]:

$$U_p(y^*, n) = U_{max}[1-(|1-2\beta y|)^{(n+1)/n}] \quad \text{(where } 0 \le y \le H/b \text{ and } \beta = b/H) \tag{1}$$

where U_{max} is the maximum velocity, which is related to the average velocity (U_{avg}) as

$$U_{max} = \left(\frac{2n+1}{n+1}\right) U_{avg} \tag{2}$$

The continuity and momentum equations for this flow system in their compact form are written as follows:

$$\text{Continuity equation: } \nabla \cdot \mathbf{U} = 0 \tag{3}$$

$$\text{Momentum equation: } \rho\left(\frac{\partial \mathbf{U}}{\partial t} + \mathbf{U}\cdot\nabla\mathbf{U} - f\right) - \nabla\cdot\sigma = 0 \tag{4}$$

where ρ, **U**, f and σ are the density, velocity vector (u^* and v^* components in Cartesian coordinates), body force, and the stress tensor, respectively.

The stress tensor, sum of the isotropic pressure (p) and the deviatoric stress tensor (τ), is given as

$$\sigma = -p\mathbf{I} + \tau \tag{5}$$

For incompressible fluids, the extra stress tensor is related to the rate of deformation tensor as

$$\tau = 2\eta\varepsilon \tag{6}$$

where ε, the component of the rate of stress tensor, is given by

$$\varepsilon = \frac{1}{2}[(\nabla\mathbf{U}) + (\nabla\mathbf{U})^T] \tag{7}$$

For power-law fluids, the viscosity (η) is defined as

$$\eta = m\left(\frac{I_2}{2}\right)^{\frac{(n-1)}{2}} \qquad \text{where } I_2 = 2(\varepsilon:\varepsilon) \tag{8}$$

where m is the power-law consistency index, n is the power-law index of the fluid (n<1, n=1 and n>1 represent the shear-thinning, Newtonian and shear-thickening fluids, respectively) and I_2 is the second invariant of the rate of strain tensor (ε). The components of the rate of strain tensor are related to the velocity components (u^* and v^*) and their derivatives, and are available in standard text books [38].

The physically realistic boundary conditions for this flow system may be written as follows:

• **At the inlet boundary**: The fully developed flow condition is imposed as

$$u^* = U_p(y^*, n) \text{ and } v^* = 0 \tag{9}$$

• **On the surface of the triangular cylinder:** The standard no-slip condition is used,

$$u^* = 0 \text{ and } v^* = 0 \tag{10}$$

• **On the top and bottom wall boundaries:** The stationary wall no-slip flow condition is imposed,

$$u^* = 0 \text{ and } v^* = 0 \tag{11}$$

• **At the exit boundary:** The default outflow boundary condition option in Fluent (a zero diffusion flux for all flow variables) is used in this work (Srikanth et al. [31] and others). This is similar to the homogeneous Neumann condition:

$$\frac{\partial u^*}{\partial x^*} = 0 \text{ and } \frac{\partial v^*}{\partial x^*} = 0 \tag{12}$$

The above equations (Eqs. (1)-(8)) along with the above noted

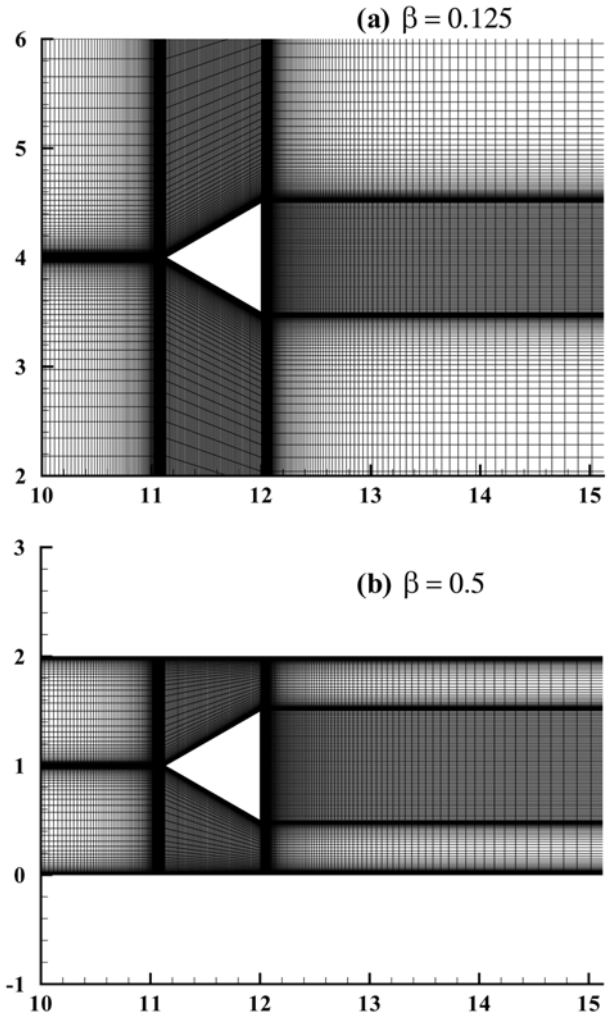

Fig. 2. Non-uniform computational grid structures around a confined triangular cylinder for the two extreme values of blockage ratio: (a) β=0.125 and (b) β=0.5.

boundary conditions (Eqs. (9)-(12)) are solved for the fluid flow around a long equilateral triangular obstacle to obtain velocity and pressure fields and so forth.

NUMERICAL METHODOLOGY

In this study, the grid structure is identical to that used recently for the confined flow and heat transfer past a triangular cylinder in a channel (Srikanth et al. [31]) and is generated by using Gambit. Figs. 2(a), (b) present the grid structure for the two extreme values of β of 0.125 and 0.5 used in this work. In brief, the grid structure consists of both uniform and non-uniform grid distributions having a fine grid in the region of larger gradients and coarse grid in the region of smaller gradients. The computational grid consists of 94794 cells, and each side of the equilateral triangular cylinder has 100 grid points with a very fine grid size of 0.002b used near the triangular cylinder and near the top and bottom walls of the channel for the blockage ratio of 0.25. The grid dependent study for the blockage ratio of 0.25 is reported in Srikanth et al. [31]. The grids of cell sizes of 104500 and 54600 are found to be adequate for the blockage ratios of 0.125 and 0.5, respectively. The problem under consideration is solved by using a commercial CFD solver Fluent (6.3). The 2-D, steady/unsteady, laminar, segregated solver is employed to solve the incompressible flow on the collocated grid arrangement. The constant density and non-Newtonian power-law viscosity models are also used. In addition, the fully developed velocity profile at the channel inlet is incorporated by using user-defined functions available in Fluent. The SIMPLE (semi implicit method for pressure linked equations) algorithm is applied to resolve the pressure-velocity coupling in conjunction with an alternating direction implicit (ADI) scheme for performing the time evolution. The second order implicit time-integration method is used here and the dimensionless time step is set to 0.01 as the smaller value of the time step did not produce any significant change in the values of the physical parameters considered in this work. The second-order upwind scheme is used to discretize convective terms, while diffusive and non-Newtonian terms have been discretized using central difference scheme. The resulting algebraic equations are solved by Gauss-Siedel iterative scheme. The residuals of the continuity, x- and y-components are used of the order of 10^{-10} in the steady state regime and of 10^{-20} in the unsteady state regime. Based upon our earlier studies (Srikanth et al. [31]; Dhiman and Shyam [39]) and based upon literature (Abbassi et al. [25,26]; De and Dalal [27]), the upstream and downstream distances of 12b and 20b, respectively, are used in this study. For instance, the effects of upstream distance on the values of the physical parameters for the Newtonian fluids are reported for X_u=10b, 12b, 14b and 40b for the lowest value of the Reynolds number of unity for β of 0.25 in our recent study [31]. Similarly, the effects of downstream distance are investigated for X_d=18b, 20b and 22b for the value of the Reynolds number of 80 [31].

RESULTS AND DISCUSSION

In the present work, numerical computations are carried out for Re=1, 5, 10, 20, 30, 40 and n=0.4, 0.6, 1, 1.4, 1.8 (shear-thinning, Newtonian and shear-thickening behaviors) for three values of β= 0.125, 0.25, 0.5 for the 2-D flow of an incompressible power-law fluids in a horizontal plane channel with a long triangular cylinder placed symmetrically on the centerline.

The numerical solution procedure used here has already been benchmarked with the standard results for the Newtonian fluid flow and heat transfer around a confined equilateral triangular cylinder in a channel and is reported elsewhere [31]. However, for the unsteady unconfined flow around an equilateral triangular cylinder, the validation of the flow and heat transfer results with literature values is documented in Dhiman and Shyam [39]. An excellent agreement is found between the present results and the literature values. Unfortunately, there are no previous results available in the literature in the case of confined flow of non-Newtonian power-law fluids around a triangular cylinder under the range of conditions studied. The following subsections present the details on the flow patterns around the long confined triangular obstacle, variation of wake/recirculation length, individual and overall drags, the variation of pressure coefficient and so forth.

1. Flow Patterns

Table 1 presents the nature of the flow as steady and/or (periodic) unsteady flow regimes. For instance, shear-thickening fluids (n>1) always display steady flow over the entire range of blockage ratio and Reynolds number considered in this work; however, shear-thinning fluids (n<1) show periodic unsteady behavior for the range 30≤Re≤40 and for Re=20 (at n=0.4) at different values of β. The flow is also found to be (periodic) unsteady at Re=40 for n=1 for the fixed value of the blockage ratio of 0.125. The unsteady nature is confirmed by carrying out the time dependent calculations in the full computational domain. But the objective here is not to investigate the transition from steady to unsteady regime.

The representative streamline contours are shown in Figs. 3-5(a)-(i) in the vicinity of the long triangular cylinder for the values of

Table 1. Nature of flow patterns: steady and unsteady flow regimes

Reynolds number, Re	Blockage ratio, BR	n=1.8	n=1.4	n=1.0	n=0.6	n=0.4
Re=1	BR=0.125	S	S	S	S	S
	BR=0.25	S	S	S	S	S
	BR=0.5	S	S	S	S	S
Re=5	BR=0.125	S	S	S	S	S
	BR=0.25	S	S	S	S	S
	BR=0.5	S	S	S	S	S
Re=10	BR=0.125	S	S	S	S	S
	BR=0.25	S	S	S	S	S
	BR=0.5	S	S	S	S	S
Re=20	BR=0.125	S	S	S	S	S
	BR=0.25	S	S	S	S	S
	BR=0.5	S	S	S	S	US
Re=30	BR=0.125	S	S	S	US	US
	BR=0.25	S	S	S	US	US
	BR=0.5	S	S	S	US	US
Re=40	BR=0.125	S	S	US	US	US
	BR=0.25	S	S	S	US	US
	BR=0.5	S	S	S	US	US

where, S=steady state, US=unsteady state

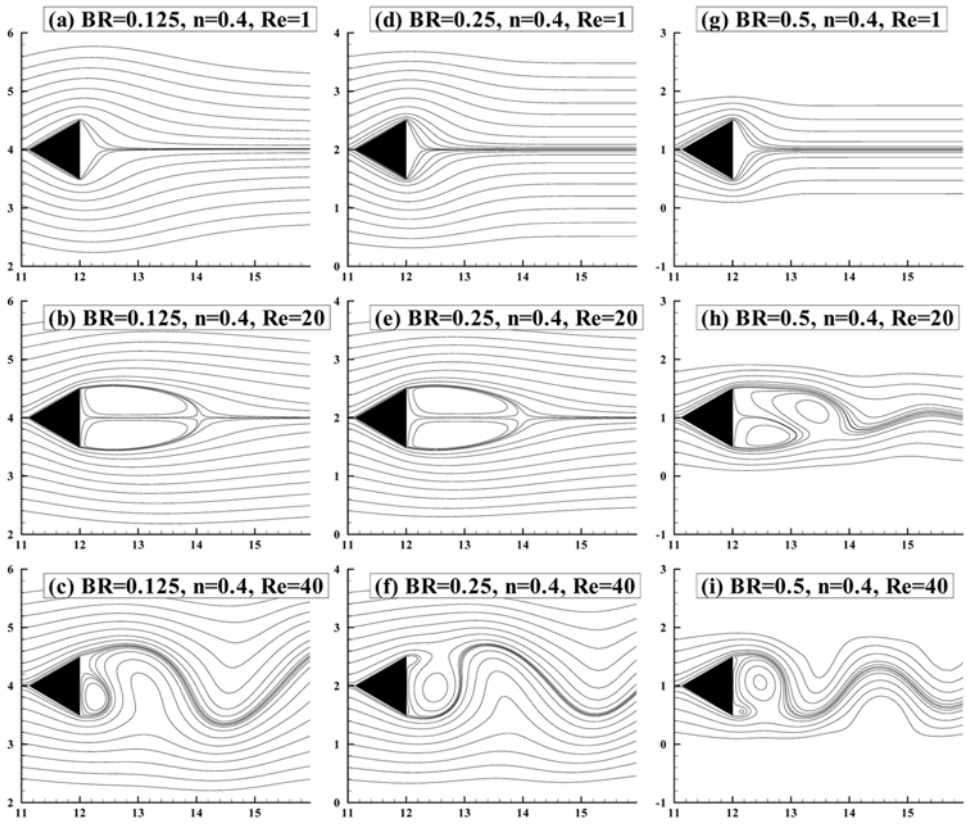

Fig. 3. Streamline contours for Re=1-40 at different values of β for shear-thinning fluids (n=0.4).

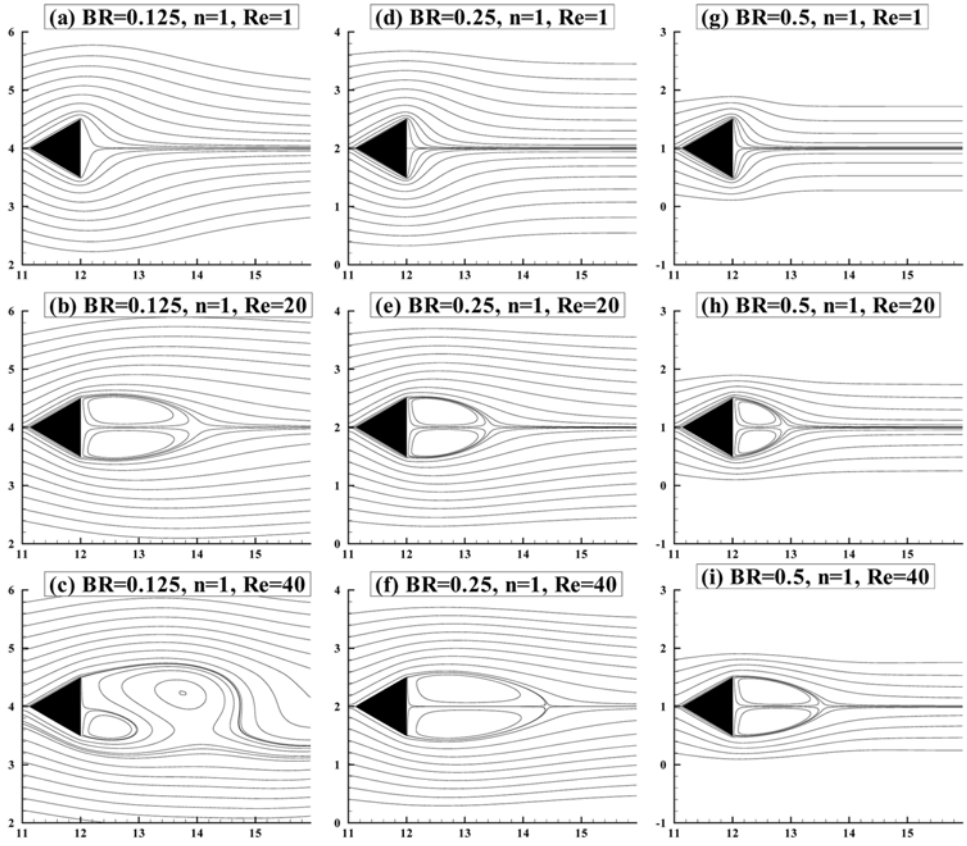

Fig. 4. Streamline contours for Re=1-40 at different values of β for Newtonian fluids (n=1).

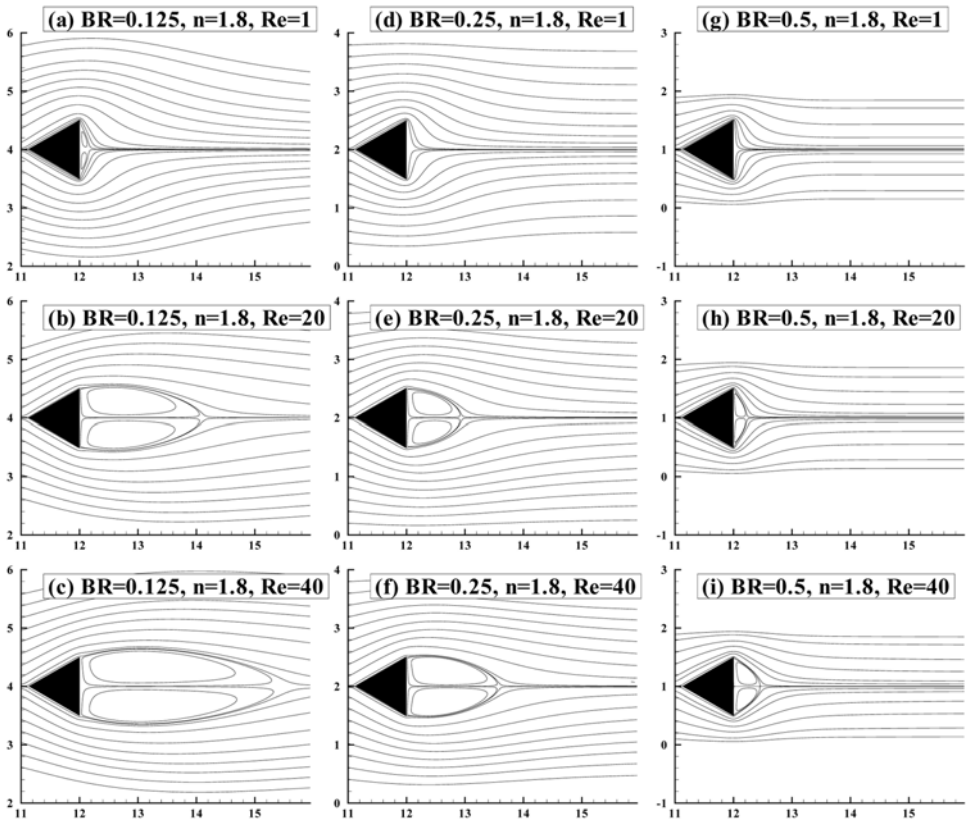

Fig. 5. Streamline contours for Re=1-40 at different values of β for shear-thickening fluids (n=1.8).

blockage ratio (β=0.125, 0.25 and 0.5) at different values of Reynolds number (at Re=1, 20 and 40) for shear-thinning (n=0.4), Newtonian (n=1) and shear-thickening (n=1.8) fluids, respectively, in the confined cross-flow regime. For a fixed value of the Reynolds number (i.e., at Re=1), no flow separation from the surface of the triangular obstacle is observed for the values of blockage ratio (β= 0.125, 0.25 and 0.5) at different values of flow behavior index (n= 0.4, 1.0 and 1.8) as the viscous force dominates the flow here. In other words, a creeping type flow is observed at Re=1 for the above range of situations. As the Reynolds number is gradually increased (1<Re≤40), the flow separates at the trailing edge of the triangular cylinder and forms two standing symmetric vortices behind the rear side of the triangular cylinder (i.e., separated flow region). This is because at high values of Re, the viscous characteristics are of little relevance as the inertial forces outweigh the viscous forces. For a fixed value of the Reynolds number, the size of the wake region decreases with increase in blockage ratio (except Re=5 and 10 for n=0.4) due to the highly non-linear nature of the viscosity of power-law fluids at n=0.4. The wake region also decreases with increase in power-law index for a fixed value of the Reynolds number for β=0.25 and 0.5; however, an opposite behavior is observed for the blockage ratio of 0.125 at different values of n (except Re=1 and 20). Qualitatively, similar dependence of the wake region on Re and n has also been reported by Dhiman et al. [17] for the non-Newtonian power-law fluid flow across a square obstacle in the unconfined steady regime. It is also observed that Newtonian and shear-thickening fluids show steady behavior with symmetric vortices (except for Newtonian fluid at Re=40 for β=0.125), but symmetric behavior disappears and the flow becomes periodic unsteady in the case of shear-thinning fluids (0.4≤n≤0.6) for the Reynolds numbers of 30 and 40 for the entire range of the values of blockage ratio studied.

2. Variation of Recirculation Length

In this work, the wake/recirculation length is measured from the rear surface of the triangular obstacle to the point of attachment for the near closed streamline (i.e., ψ=0) on the axis of symmetry. The location of the attachment point is determined computationally by monitoring the streamwise velocity along the streamwise centerline of the triangular cylinder and moving downstream until its sign changes from negative to positive.

The variation of the nondimensional recirculation length (L_r/b) as a function of Reynolds number, power-law index and blockage ratio is shown in Figs. 6(a)-(c). For the steady confined flow regime, the recirculation length increases with increasing value of the Reynolds number for a fixed value of the blockage ratio. This is because at low values of Re, fluid elements are able to follow closely the contour of the cylinder; whereas at high values of Re, there exists separation of the flow from the cylinder. For a fixed value of the Reynolds number, the wake length decreases with increase in blockage ratio (except Re=5 and 10 for n=0.4) due to the highly non-linear nature of the viscosity of power-law fluids at n=0.4. The size of the wake length also decreases with increase in power-law index for a fixed value of the Reynolds number for β=0.25 and 0.5; however, the opposite behavior is observed for the blockage ratio of 0.125 at different values of n (except Re=1 and 20). The reverse trend in the variation of the wake length is a characteristic feature of the un-

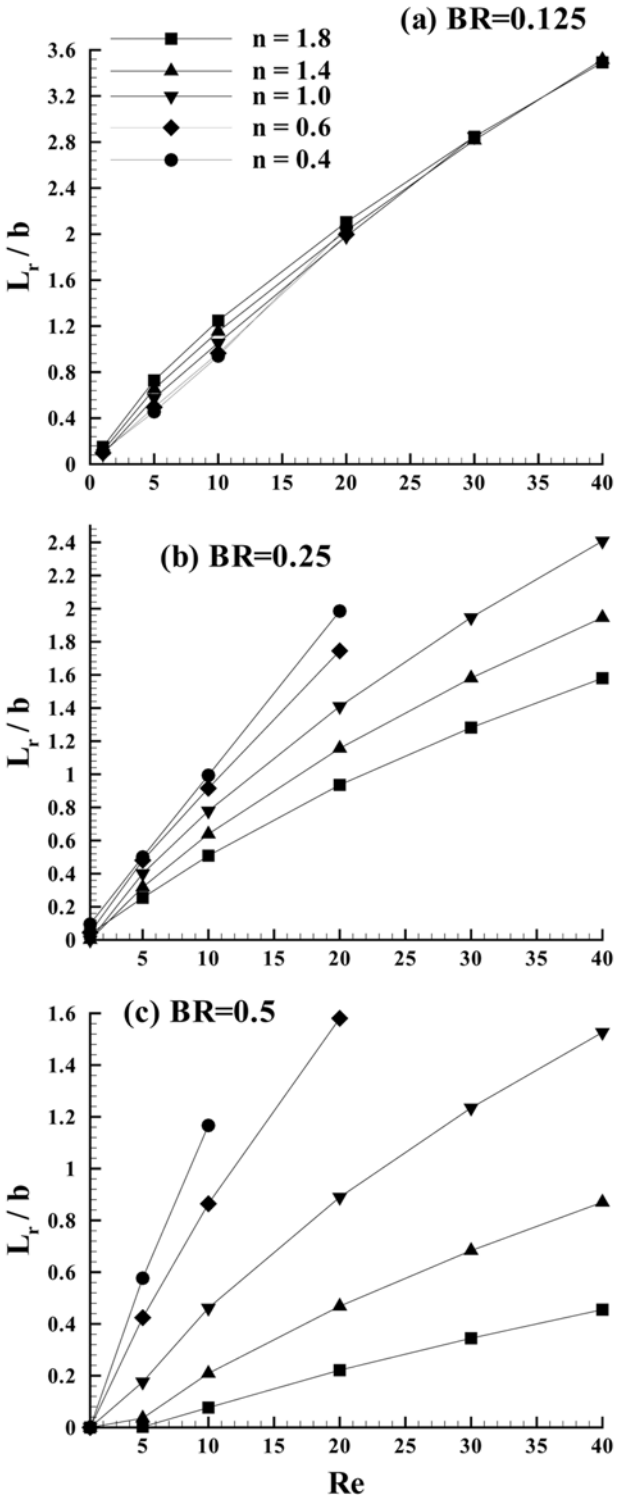

Fig. 6. Variation of wake length with Reynolds number, blockage ratio and power-law index in the steady regime: (a) β= 0.125, (b) β=0.25 and (b) β=0.5.

confined flow, irrespective of the power-law index. Broadly, the wake length of Newtonian fluid (n=1) is found to be more than the shear-thickening fluids (n>1), but less than the shear-thinning fluids (n<1) for the values of blockage ratio of 0.25 and 0.5. While the opposite trend of the recirculation length of Newtonian fluid is observed for the blockage ratio of 0.125. Similar reliable results have also been reported by Dhiman et al. [17] for the power-law fluids in the unconfined region for the long square obstacle. Furthermore, the following simple Newtonian correlation can be used for the calculation of wake length for the intermediate values of Re and β:

$$L_r/b=A+B(\beta Re)+C(\beta Re)^2 \quad (13)$$

The corresponding values of the fitted constants (A, B and C) along with their maximum and average deviations are given in Table 2. Fourteen data points are being used in developing the above correlation.

3. Individual and Overall Drag Coefficients

It is well known that the total drag force exerted by the fluid on any bluff body is made up of two components: viscous drag (C_{DF}) and pressure drag (C_{DP}). The variations of individual and overall drags (C_{DP}, C_{DF} and C_D) with Reynolds number at different values of power-law index for the entire range of blockage ratio are shown in Figs. 7(a)-(i) along with their zoomed views in the steady regime. The drag (individual and total drag coefficients) strongly depends upon Reynolds number, blockage ratio and power law-index. For the fixed values of blockage ratio and power-law index, as expected, the values of C_{DP}, C_{DF} and C_D decrease with increase in the Reynolds number. However, for a fixed value of the Reynolds number, C_{DP}, C_{DF} and C_D decrease with decrease in power-law index and/or blockage ratio in the steady confined flow regime. The influence of the power-law rheology is found to be more prominent at high values of blockage ratio (β=0.25 and 0.5, for instance). This is due to the non-linear nature of the viscosity over the surface of the triangular cylinder and/or on the confining walls. On the other hand, in the case of another sharp edge bluff body of square cross-section for the flow of power-law fluids [17], similar behavior is reported for the Re range 15<Re≤45; however, the opposite behavior is observed for the Reynolds number range Re≤15. It has also been observed that the pressure drag coefficient is always larger than the friction drag coefficient for all the values of blockage ratio studied and the corresponding power-law index for all the values of Reynolds number (except for n=1.8 (5≤Re≤40) and n=1.4 (Re=5) at β=0.125). The drag coefficient of Newtonian fluid is found to be larger than the shear-thinning fluids (n<1) and smaller than the shear-thickening fluids (n>1).

We also observed that the flow becomes unsteady periodic for shear-thinning behaviors even at low values of Reynolds number (Re≤40) at different values of blockage ratio (Table 1). In the unsteady regime, the variation of the time-averaged values of the total drag coefficient ($\overline{C}_D$) with Re (30≤Re≤40) for shear-thinning behaviors

Table 2. Correlation fitted constants (A, B and C) for determining L_r/b at various values of blockage ratio and Reynolds number

Blockage ratio, β	Reynolds number, Re	A	B	C	Average deviation (%)	Maximum deviation (%)
0.125	5≤Re≤30	0.1524	0.8662	−0.05725	1.07	3.03
0.25	5≤Re≤40	0.2132	0.6838	−0.2436	0.49	0.92
0.5	5≤Re≤40	0.2325	0.5750	−0.4113	0.19	0.32

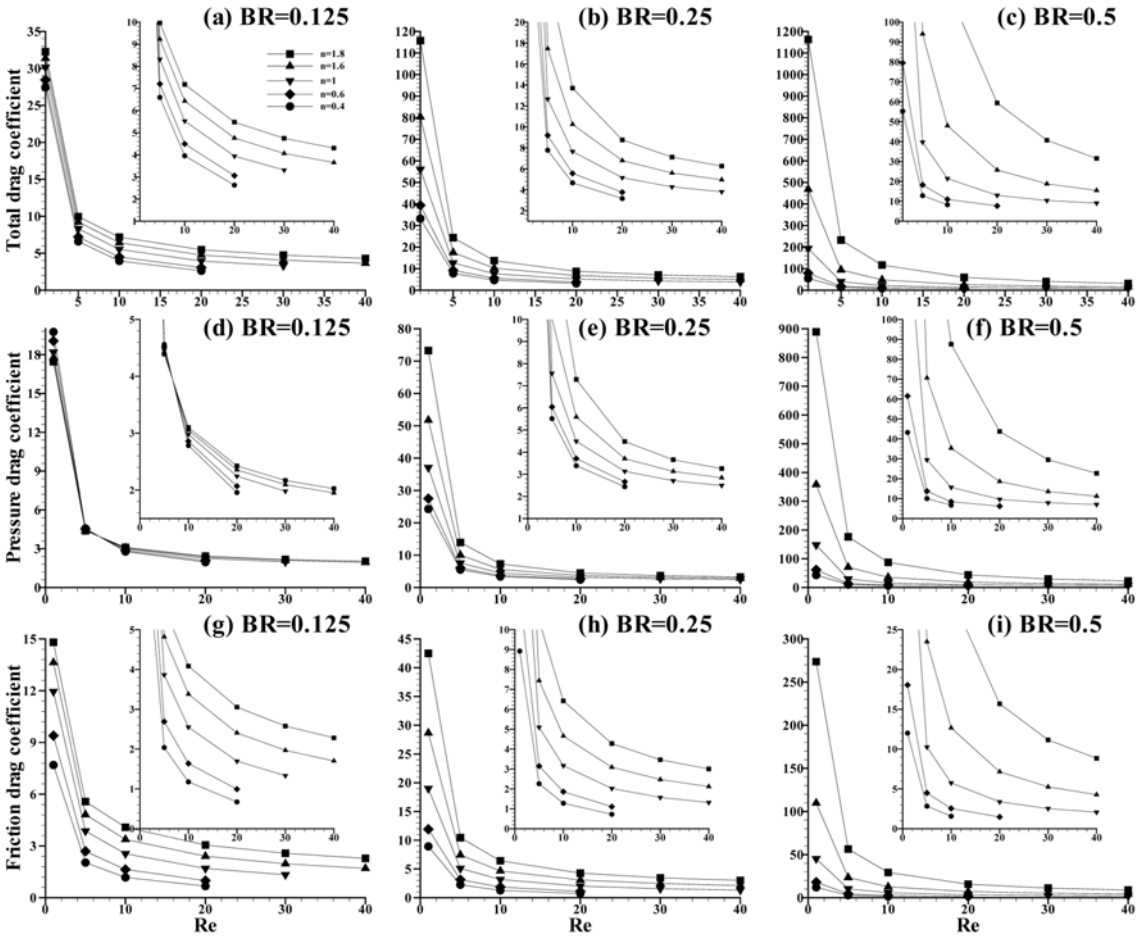

Fig. 7. Variation of (a)-(c) overall drag, (d)-(f) pressure drag and (g)-(i) friction drag coefficients at different values of Re, n and β.

Table 3. The time-averaged total drag coefficient ($\overline{C}_D$), rms values of drag (C_{Drms}) and lift (C_{Lrms}) coefficients and Strouhal number (St) with Re, n and β

β	n	Re	$\overline{C}_D$	C_{Drms}	St	C_{Lrms}
0.5	0.4	20	6.2479	0.0010	0.4742	0.1054
		30	6.1129	0.1919	0.4297	0.9116
		40	7.1188	0.5697	0.4394	1.4249
	0.6	30	6.6615	0.0027	0.4848	0.1389
		40	6.1643	0.0111	0.4722	0.2788
0.25	0.4	30	2.9336	0.0219	0.2738	0.2189
		40	4.0123	0.2680	0.3099	0.7253
	0.6	30	3.2046	0.0015	0.2654	0.0887
		40	3.2811	0.0488	0.2863	0.3646
0.125	0.4	30	2.3860	0.0058	0.2281	0.1131
		40	3.4330	0.2020	0.2788	0.6065
	0.6	30	2.6496	0.0013	0.2132	0.0784
		40	2.9465	0.0506	0.2561	0.3491
	1	40	3.0868	0.0026	0.0657	0.0923

(n<1) at different values of β as well as for Newtonian fluid (n=1 at β=0.125) is reported in Table 3. The time-averaged values of the total drag coefficient decrease with increasing Reynolds number for the values of blockage ratio of 0.25 and 0.125 in the (periodic) unsteady regime. However, for the blockage ratio of 0.5, the time-averaged drag coefficient increases with Re for n=0.6 and the mixed trend is observed for n=0.4. For a fixed value of the Reynolds number, the time-averaged drag decreases with decrease in blockage ratio and/or power-law index.

Similar to time-averaged drag, the time-averaged lift coefficient is also calculated by averaging at least ten cycles beyond the time the asymptotic shedding frequency of Kármán vortex is attained. The time-averaged lift coefficient remains approximately zero (on the order of about 10^{-3}-10^{-6}) for 20≤Re≤40 and n<1 for the entire range of blockage ratio studied here. The variation of the root mean square (rms) values of the drag and lift coefficients and the Strouhal number with Reynolds number, power-law index and blockage ratio is documented in Table 3. These rms values give a measure of the amplitude of the unsteady cylinder wake oscillations.

The Strouhal number represents the frequency of the vortex shedding in the unsteady periodic regime and defined here as St=fb/U_{avg}. The temporal variation of the lift coefficient is used to calculate the frequency of the vortex shedding (f) by using fast Fourier transformation. The value of the Strouhal number is obviously zero in the steady flow with two symmetric wakes attached to the long obstacle. The Strouhal number behaves in the similar fashion as the time-averaged drag coefficient for the range of conditions: 20≤ Re≤40 and n<1 (Table 3).

The rms value of the lift coefficient increases with increasing value

of the Reynolds number in the unsteady regime. For the fixed values of the Reynolds number and the blockage ratio, the rms value of the lift coefficient decreases with increasing power-law index. However, for the fixed values of the Reynolds number and the power-law index, the rms value of the lift coefficient decreases with decreasing blockage ratio. Similar trends are also observed for the rms value of the drag coefficient at different values of Re, β and n.

Furthermore, the total drag coefficient for the intermediate values of Reynolds number and blockage ratio can be calculated by using following Eqs. (14) and (15):

For β=0.125,

$$C_D=A+BRe^C \quad (14)$$

For β=0.25 and 0.5,

$$C_D=A+B(\beta/Re)+C(\beta/Re)^2 \quad (15)$$

The corresponding values of the fitted constants (A, B and C) along

Table 4. Correlation fitted constants (A, B and C) for determining C_D at various values of blockage ratio and Reynolds number

Blockage ratio, β	Reynolds number, Re	A	B	C	Average deviation (%)	Maximum deviation (%)
0.125	1≤Re<40	1.820	28.610	−0.892	0.65	3.70
0.25	1≤Re≤40	2.624	198.2	62.63	0.53	1.49
0.5	1≤Re≤40	4.550	342.6	70.62	1.28	2.83

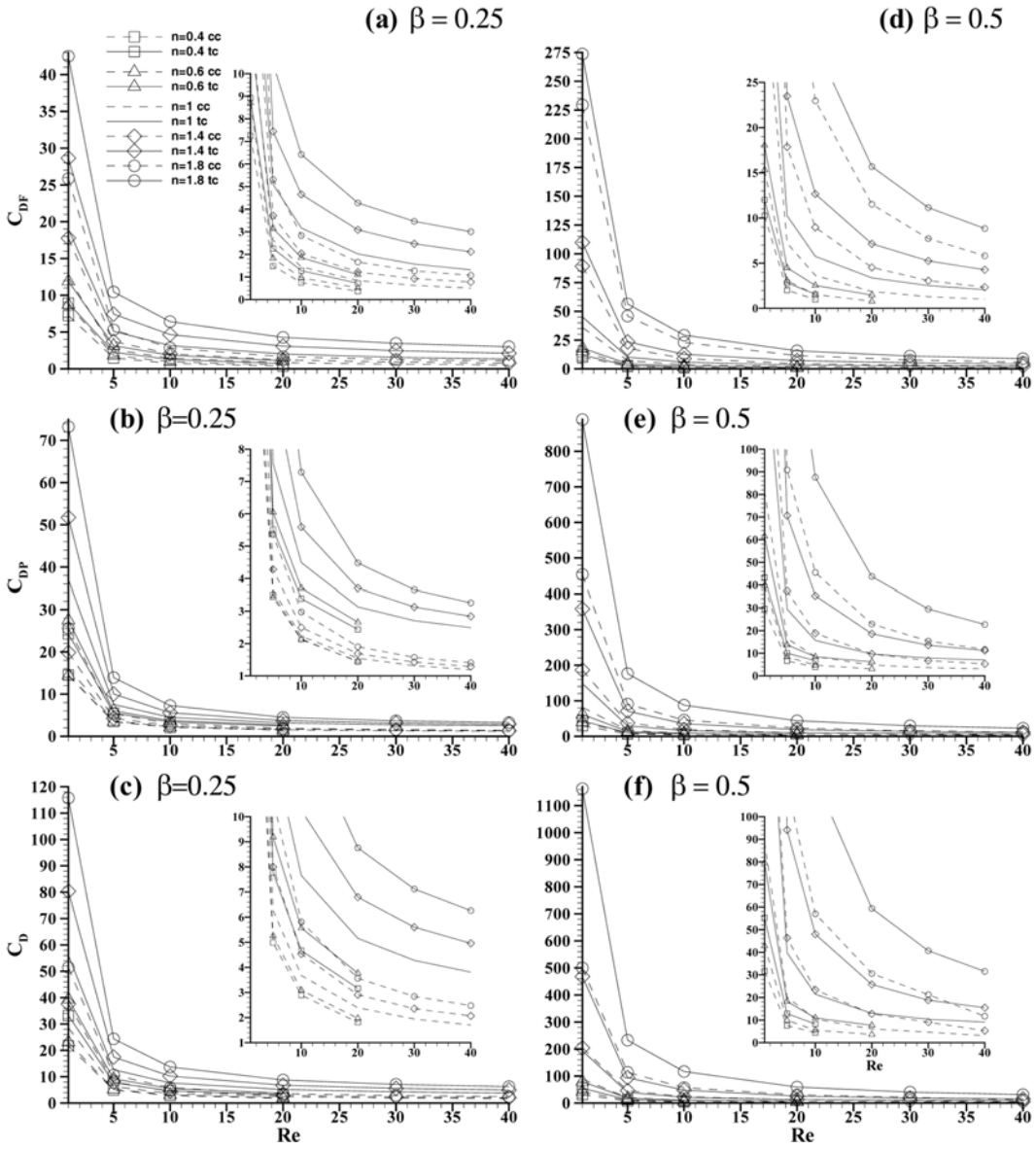

Fig. 8. Comparison of friction (a), (d), pressure (b), (e) and total drag (c), (f) coefficients of triangular cylinder with circular cylinder [10] for β=0.25 and 0.5. The dashed and solid lines are for circular cylinder (cc) and triangular cylinder (tc), respectively.

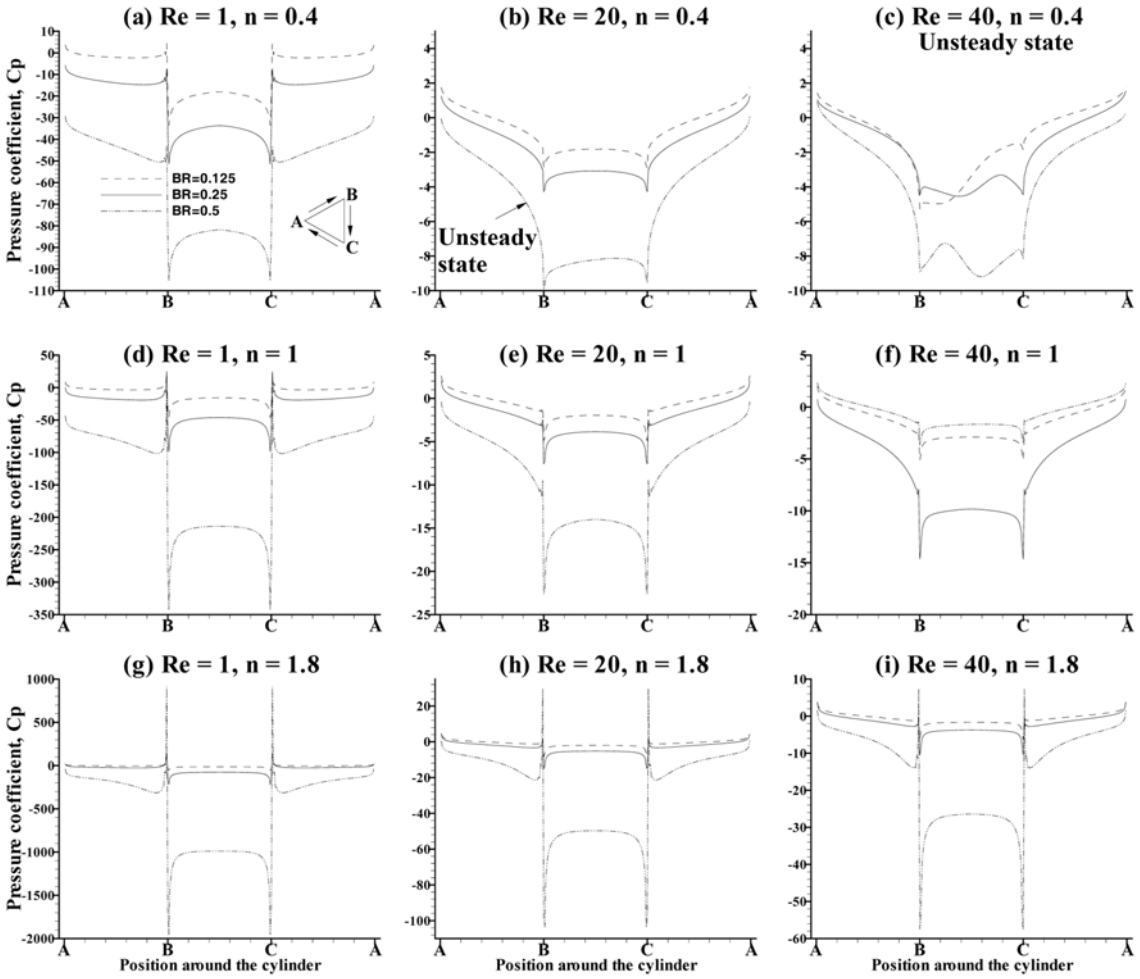

Fig. 9. Variation of pressure coefficient for Re=1 (a), (d), (g), 20 (b), (e), (h) and 40 (c), (f), (i) at different values of n and β.

with their maximum and average deviations are given in Table 4. Seventeen data points are being used in developing the above Newtonian correlation.

Next, the comparison of present triangular cylinder results with circular cylinder is presented in Figs. 8(a)-(f). Fig. 8 presents the comparison of friction, pressure and total drag coefficients for the cylinders of triangular and circular [10] cross-sections for the non-Newtonian power-law fluids (n=0.6-1.8) for the values of blockage ratio of 0.25 (Figs. 8(a)-(c)) and 0.5 (Figs. 8(d)-(f)) in the steady regime. Bharti et al. [10] investigated the flow of power-law fluids past a long circular cylinder for an extensive range of parameters (Re=1-40, n=0.2-1.9 and β=0.25-0.91) in the steady regime. For both the bluff bodies, similar trends of drag are observed at different values of Re, β and n. For instance, the individual and overall drag coefficients decrease with increasing value of the Reynolds number. However, the values of individual and overall drag coefficients for the triangular cylinder are found to be larger than that of the circular cylinder as the triangular cylinder is more bluff body than the circular one (Fig. 8).

4. Variation of Pressure Coefficient Around the Obstacle

The pressure coefficient (C_p) is defined as the ratio of the static pressure to the dynamic pressure. On the surface of the triangular obstacle, it is computed by using the following Eq. (16):

$$C_p = \frac{p_s - p_\infty}{\frac{1}{2}\rho U_\infty^2} \tag{16}$$

where p_s is the local pressure at a point on the surface of the cylinder and p_∞ is the reference pressure.

Figs. 9(a)-(i) show the variation of the pressure coefficient along the top (AB), bottom (CA) and rear (BC) surfaces of the triangular cylinder (where the apex of the cylinder is facing the upstream direction) in a channel for Re=1, 20 and 40 for the range of values of β and n. The variation of the pressure coefficient is found to be symmetric about the mid plane as the flow is steady in the steady cross-flow regime. The flow is observed to be unsteady for shear-thinning fluids (n=0.4) at Re=20, β=0.5 (Fig. 9(b)) and at Re=40, β=0.125-0.5 (Fig. 9(c)). For the fixed values of Reynolds number and power-law index, the pressure coefficient is seen to decrease from its maximum value at the front stagnant point (a point where the fluid velocity becomes zero) along the upper and lower surfaces of the triangular cylinder; however, on the rear surface of the obstacle (i.e., on BC), the pressure coefficient increases from its minimum value from the upper separation point (B) and then decreases to minimum value to the lower separation point (C). The pressure coefficient decreases with increasing value of the Reynolds number for the blockage ratio of 0.125 for all the values of n studied;

however, the pressure coefficient increases with increasing value of the Reynolds number for the blockage ratios of 0.25 and 0.5. The pressure coefficient has seen to be increased with decrease in blockage ratio for all the values of n considered. For a fixed value of the blockage ratio (β=0.125 and 0.25), the pressure coefficient increases with increasing value of the power-law index. However, for β=0.5, the pressure coefficient over the surfaces of the triangular cylinder for shear-thinning fluids is observed to be higher than Newtonian fluid and lower than shear-thickening fluids at Re=1; while in the range of Re=20-40, the pressure coefficient of Newtonian fluid is found to be higher than the shear-thinning fluids and lower than that of the shear-thickening fluids.

CONCLUSIONS

The effect of blockage ratio (β=0.125, 0.25 and 0.5) on the flow of non-Newtonian power-law fluids over a triangular cylinder conned in a planar channel has been studied for the range of values as 0.4≤ n≤1.8 and 1≤Re≤40 in the 2-D laminar flow regime. Extensive numerical results on flow patterns, wake length, individual and total drag coefficients and the variation of pressure coefficient on the surface of the long triangular cylinder are reported to elucidate the combined effects of Re, n and β. The wake length of Newtonian fluid (n=1) is found to be more than shear-thickening fluids (n>1) and less than the shear-thinning fluids (n<1) for the blockage ratios of 0.25 and 0.5; whereas, for the blockage ratio of 0.125, the recirculation length of Newtonian fluid is observed to be less than the shear-thickening and shear-thinning fluids. For a fixed value of the Reynolds number, individual and overall drags (C_{DP}, C_{DF} and C_D) decrease with decrease in power-law index and/or blockage ratio in the steady flow regime. The pressure coefficient increases with increasing value of the blockage ratio for all the values of power-law index covered here. Finally, simple correlations of wake length and drag are obtained for the above range of settings.

NOMENCLATURE

b : side of an equilateral triangular cylinder [m]
C_D : total drag coefficient, $C_D = \frac{2F_D}{\rho U_{avg}^2 b}$
$\overline{C}_D$: time-averaged drag coefficient, dimensionless
C_{DF} : friction component of drag coefficient, $C_{DF} = \frac{2F_{DF}}{\rho U_{avg}^2 b}$
C_{DP} : pressure component of drag coefficient, $C_{DP} = \frac{2F_{DP}}{\rho U_{avg}^2 b}$
C_{Drms} : rms value of the drag coefficient, dimensionless
C_L : total lift coefficient, $C_L = \frac{2F_L}{\rho U_{avg}^2 b}$
C_{Lrms} : rms value of the lift coefficient, dimensionless
C_p : pressure coefficient, dimensionless
f : vortex shedding frequency [s^{-1}]
F_D : drag force per unit length of the cylinder [N m^{-1}]
F_{DF} : frictional component of the drag force per unit length of the cylinder [N m^{-1}]
F_{DP} : pressure component of the drag force per unit length of the cylinder [N m^{-1}]
F_L : lift force per unit length of the cylinder [N m^{-1}]
H : height of the computational domain [m]
I_2 : second invariant of the rate of the strain tensor [s^{-2}]
L : length of the computational domain [m]
L_r : wake/recirculation length [m]
m : power-law consistency index [Pa s^n]
n : power-law index, dimensionless
p : pressure [Pa]
p_0 : free stream pressure [Pa]
Re : Reynolds number, $Re = \frac{\rho U_{avg}^{2-n} b^n}{m}$
St : Strouhal number, $St = \frac{fb}{U_{avg}}$
t : time [s]
u : component of the velocity in the x-direction, $u = u^*/U_{avg}$
U_{avg} : average velocity at the channel inlet [ms^{-1}]
U_{max} : maximum velocity at the channel inlet [ms^{-1}]
U_p : fully developed velocity of the fluid [ms^{-1}]
v : component of the velocity in the y-direction, $v = v^*/U_{avg}$
x : stream-wise coordinate, $x = x^*/b$
y : transverse coordinate, $y = y^*/b$
X_d : downstream distance of the cylinder [m]
X_u : upstream distance of the cylinder [m]

Greek Symbols

β : blockage ratio, BR (=b/H)
η : viscosity of the fluid [Pa·s]
ρ : density of the fluid [kg m^{-3}]
ε : component of the rate of strain tensor [s^{-1}]
τ : extra stress tensor [Pa]
ψ : stream function [m^2 s^{-1}]

Superscript

* : dimensional variable

REFERENCES

1. R. P. Chhabra and J. F. Richardson, *Non-newtonian flow in the process industries*, Butterworth-Heinemann, Oxford (1999).
2. R. P. Chhabra, Bubbles, Drops and Particles in Non-Newtonian Fluids, second Ed., CRC Press, Boca Raton, FL (2006).
3. S. J. D. D'Alessio and J. P. Pascal, *Acta Mechanica*, **117**, 87 (1996).
4. R. P. Chhabra, A. A. Soares and J. M. Ferreira, *Acta Mechanica*, **172**, 1 (2004).
5. S. J. D. D'Alessio and L. A. Finlay, *Ind. Eng. Chem. Res.*, **43**, 8407 (2004).
6. A. A. Soares, J. M. Ferreira and R. P. Chhabra, *Ind. Eng. Chem. Res.*, **44**, 5815 (2005).
7. W. A. Khan, J. R. Culham and M. M. Yovanovich, *J. Heat Transfer*, **128**, 870 (2006).
8. R. P. Bharti, R. P. Chhabra and V. Eswaran, *Canadian J. Chem. Eng.*, **84**, 406 (2006).
9. R. P. Bharti, R. P. Chhabra and V. Eswaran, *Int. J. Heat Mass Transfer*, **50**, 977 (2007).
10. R. P. Bharti, R. P. Chhabra and V. Eswaran, *Ind. Eng. Chem. Res.*, **46**, 3820 (2007).

11. P. Sivakumar, R. P. Bharti and R. P. Chhabra, *Chem. Eng. Sci.*, **61**, 6035 (2006).
12. M. J. Shah, E. E. Petersen and A. Acrivos, *AIChE J*., **8**, 542 (1962).
13. P. M. Coelho and F. T. Pinho, *J. Non-Newtonian Fluid Mech.*, **110**, 143 (2003).
14. P. M. Coelho and F. T. Pinho, *J. Non-Newtonian Fluid Mech.*, **110**, 177 (2003).
15. P. M. Coelho and F. T. Pinho, *J. Non-Newtonian Fluid Mech.*, **121**, 55 (2004).
16. V. K. Patnana, R. P. Bharti and R. P. Chhabra, *Chem. Eng. Sci*., **64**, 2978 (2009).
17. A. K. Dhiman, R. P. Chhabra and V. Eswaran, *Chem. Eng. Res. Design*, **84A**, 300 (2006).
18. A. K. Dhiman, N. Anjaiah, R. P. Chhabra and V. Eswaran, *Trans. ASME J. Fluids Eng.*, **129**, 506 (2007).
19. A. K. Dhiman, R. P. Chhabra and V. Eswaran, *J. Non-Newtonian Fluid Mech*., **148**, 141 (2008).
20. Akhilesh K. Sahu, R. P. Chhabra and V. Eswaran, *J. Non-Newtonian Fluid Mech*., **160**, 157 (2009).
21. A. K. Sahu, R. P. Chhabra and V. Eswaran, *J. Non-Newt. Fluid Mech*., **165**, 752 (2010).
22. P. Koteswara Rao, A. K. Sahu and R. P. Chhabra, *Int. J. Heat Mass Transfer*, **54**, 390 (2011).
23. Mohamed Bouaziz, Sameh Kessentini and Saïd Turki, *Int. J. Heat Mass Transfer*, **53**, 5420 (2010).
24. A. Prhashanna, A. K. Sahu and R. P. Chhabra, *Int. J. Therm. Sci.*, **50**, 2027 (2011).
25. H. Abbassi, S. Turki and S. Ben Nasrallah, *Numerical Heat Transfer, Part A*, **39**, 307 (2001).
26. H. Abbassi, S. Turki and S. Ben Nasrallah, *Int. J. Therm. Sci*., **40**, 649 (2001).
27. A. K. De and A. Dalal, *ASME J. Heat Transfer*, **129**, 646 (2007).
28. Himadri Chattopadhyay, *Int. J. Therm. Sci.*, **46**, 501 (2007).
29. A. K. Dhiman and S. Srikanth, Steady state flow across a triangular cylinder placed in a channel, 62nd Annual Session of Indian Chemical Engineering Congress, CHEMCON 2009, Dept. of Chemical Eng., Andhra University, Viskhapatnam, India, Dec. 27-30 (2009).
30. Mousa Farhadi, Kurosh Sedighi and Afshin Mohsenzadeh Korayem, *Int. J. Therm. Sci*., **49**, 1010 (2010).
31. S. Srikanth, A. K. Dhiman and S. Bijjam, *Int. J. Therm. Sci*., **49**, 2191 (2010).
32. Mohamed Ali, O. Zeitoun and A. Nuhait, *Int. J. Therm. Sci*., **50**, 106 (2011).
33. A. K. De and A. Dalal, *Int. J. Numerical Methods Fluids*, **52**, 801 (2006).
34. A. Dalal, V. Eswaran and G. Biswas, *Numer. Heat Transfer B*, **54**, 238 (2008).
35. Amit Kumar Dhiman, Fluid flow and heat transfer across a triangular cylinder, Proc. 20th National and 9th ISHMT-ASME Heat and Mass Transfer Conference, Paper No: 10HMTC185, Indian Institute of Technology Mumbai, India, Jan. 4-6 (2010).
36. Amit Kumar Dhiman and Radhe Shyam, Unsteady heat transfer across a triangular cylinder, Proc. 20th National and 9th ISHMT-ASME Heat and Mass Transfer Conference, Paper No: 10HMTC260, Indian Institute of Technology Mumbai, India, Jan. 4-6 (2010).
37. O. Zeitoun, Mohamed Ali and A. Nuhait, *Int. J. Therm. Sci*., **50**, 1685 (2011).
38. R. B. Bird, W. E. Stewart and E. N. Lightfoot, Transport Phenomena, Second Ed., Wiley, New York (2002).
39. Amit Dhiman and Radhe Shyam, *ISRN Mech. Eng*., **2011**, 1 (2011).